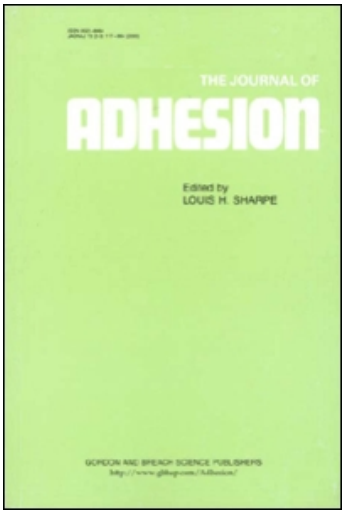

The Journal of Adhesion
Publication details, including instructions for authors and subscription information:
http://www.informaworld.com/smpp/title~content=t713453635

The Fatigue and Durability Behaviour of Automotive Adhesives. Part II: Failure Mechanisms

R. A. Dickie[a]; L. P. Haack[a]; J. K. Jethwa[bc]; A. J. Kinloch[b]; J. F. Watts[d]
[a] Ford Research Laboratory, Ford Motor Company, Dearborn, MI, USA [b] Department of Mechanical Engineering, Imperial College of Science, Technology and Medicine, London, UK [c] Autoliv, Havant, Hampshire, UK [d] Department of Materials Science and Engineering, University of Surrey, Guildford, Surrey, UK

To cite this Article Dickie, R. A. , Haack, L. P. , Jethwa, J. K. , Kinloch, A. J. and Watts, J. F.(1998) 'The Fatigue and Durability Behaviour of Automotive Adhesives. Part II: Failure Mechanisms', The Journal of Adhesion, 66: 1, 1 — 37
To link to this Article: DOI: 10.1080/00218469808009958
URL: http://dx.doi.org/10.1080/00218469808009958

J. Adhesion, 1998, Vol. 66, pp. 1 - 37
Reprints available directly from the publisher
Photocopying permitted by license only

The Fatigue and Durability Behaviour of Automotive Adhesives. Part II: Failure Mechanisms

R. A. DICKIE[a], L. P. HAACK[a], J. K. JETHWA[b,*],
A. J. KINLOCH[b,**] and J. F. WATTS[c]

[a]*Ford Research Laboratory, Ford Motor Company, PO Box 2053, MD 3083 SRL, Dearborn, MI 48121-2053, USA;* [b]*Department of Mechanical Engineering, Imperial College of Science, Technology and Medicine, Exhibition Rd., London, SW7 2BX, UK;* [c]*Department of Materials Science and Engineering, University of Surrey, Guildford, Surrey, GU2 5XH, UK*

(Received 10 June 1997; In final form 19 August 1997)

In part I [1] a fracture mechanics approach has been successfully used to examine the cyclic fatigue behaviour of adhesively-bonded joints, which consisted of aluminium-alloy or electro-galvanised (EG) steel substrates bonded using toughened-epoxy structural paste-adhesives. The adhesive systems are typical of those being considered for use, or in use, for bonding load-bearing components in the automobile industry. The cyclic fatigue tests were conducted in a relatively dry environment, of 23°C and 55% RH, and in a "wet" environment, namely immersion in distilled water at 28°C. The "wet" fatigue tests clearly revealed the significant effect an aggressive, hostile environment may have upon the mechanical performance of adhesive joints, and highlighted the important influence that the surface pretreatment, used for the substrates prior to bonding, has upon joint durability. The present paper, Part II, discusses the modes and mechanisms of failure for the two adhesive systems in both the "dry" and "wet" environments. The failure surfaces of the joints tested in Part I have been examined using a variety of analytical techniques and the surface chemistry and morphology compared with that of the "as prepared" (i.e. non-bonded) metal surfaces and cured adhesive. In the present investigation use has been made of an elemental mapping form of X-ray photoelectron spectroscopy (EM-XPS) along with conventional XPS. The surface topography has been examined using scanning electron microscopy and atomic force microscopy. Also, cross-sections of the joints have been studied using the transmission electron microscope. The results reveal that for both the aluminium alloy and EG steel joints that the failure path is complex, and is associated with electrochemical activity (i.e. corrosion) in the case of the latter

*Present address: Autoliv, Penner Rd., Havant, Hampshire, PO9 1QH, UK.
**Corresponding author.

joints when tested in the "wet" environment. In part III [2], the results presented in the earlier papers will be used to predict the lifetime of single-overlap joints subjected to cyclic fatigue loading.

Keywords: Aluminium alloy; automotive applications; durability; electro-galvanised steel; electron microscopy; fatigue; fracture mechanics; structural adhesives; surface analysis; surface pretreatments

1. INTRODUCTION

The present research is particularly directed towards adhesives for automotive applications. Adhesives are currently used in many areas in the manufacture of automobiles, but almost always either as basically sealant materials or in non-critical secondary structures. So far the use of adhesives in truly structural applications has been very limited. A major reason for this has been a concern about the fatigue and durability behaviour of bonded, structural components over the expected lifetime of the vehicle. This concern arises since the adhesive joints must perform satisfactorily under service conditions which include dynamically applied loads and exposure to hostile environments such as water, road salt, petrol, other organic solvents, etc.; and, in many instances, combinations of these conditions may be experienced [3, 4].

In Part I [1] a fracture mechanics approach has been successfully used to examine the cyclic fatigue behaviour of adhesively-bonded joints, which consisted of aluminium-alloy or electro-galvanised (EG) steel substrates bonded using toughened-epoxy structural paste-adhesives. The adhesive systems are typical of those being considered for use, or in use, for bonding load-bearing components in the automobile industry. The two adhesives employed were (i) a one-part epoxy-paste adhesive, Grade "XD4600" supplied by Ciba Polymers, UK, developed especially for bonding aluminium alloys; and (ii) a one-part epoxy-paste, Grade "Terokal 4520-34" supplied by Teroson, which is currently being used to bond EG steel parts for the automobile industry. In the case of the aluminium-alloy, before bonding the substrates were either grit-blasted and solvent degreased (GBD), or subjected to a chromic-acid etch (CAE). In the case of the EG steel, the substrates were simply solvent degreased using 1,1,1 trichloroethane.

The cyclic fatigue results were plotted in the form of the rate of crack growth per cycle, *da/dN*, *versus* the maximum strain-energy release rate, G_{max}, applied in the fatigue cycle, using logarithmic axes. Of particular interest was the presence of a threshold value of the strain-energy release rate, G_{th}, applied in the fatigue cycle, below which fatigue crack growth was not observed to occur. The cyclic fatigue tests conducted in a relatively dry environment of 23°C and 55% r.h. were shown to cause crack propagation at far lower values of G_{max} compared with the value of the adhesive fracture energies, G_c, which were determined from monotonically-loaded fracture tests. Cyclic fatigue tests were also conducted in a "wet" environment, namely immersion in distilled water at 28°C. The "wet" fatigue tests clearly revealed the further significant effect an agressive, hostile environment may have upon the mechanical performance of adhesive joints, and highlighted the important influence that the surface pretreatment, used for the substrates prior to bonding, has upon joint durability. The locus of joint failure was visually assessed. The main results from the work reported in Part I are summarised in Table I below.

In the present paper, Part II, the locus of failure of the joints and the mechanisms of environmental attack are considered. Over the last two

TABLE I Summary of main results from Part I [1]

Joint type	*Monotonic Tests*		*Fatigue tests*	
	$G_c(J/m^2)$	*LoF*	$G_{th}(J/m^2)$	*LoF*
Aluminium-alloy/ "XD4600" joints				
"Dry" environment:				
Grit-blast/degreased	3000	C/IF[a]	250	C/IF
Chromic-acid etch	3500	C	355	C
"Wet" environment:				
Grit-blast/degrease	–	–	80	IF
Chromic-acid etch	–	–	200	IF
EG steel/ "Terokal 4520-34" joints				
"Dry" environment:				
Degreased	740	C	240	C
"Wet" environment:				
Degreased	–	–	140	IF

[a]LoF: locus of joint failure, visually addressed.
C: cohesive in the adhesive layer.
IF: interfacial between the adhesive and substrate.

decades X-ray photoelectron spectroscopy (XPS) has established itself as the method of choice for the detailed investigation of the interfacial chemistry of failed adhesive joints and organic coatings. The advantages of XPS are well known but include the ability to accommodate insulating samples, the provision of a quantitative surface analysis of all elements of the periodic table with the exception of hydrogen, and the chemical state information that can be obtained by way of the XPS chemical shift. This enables the adhesion scientist to identify aspects such as (i) the degradation of both the polymeric phase and the metal substrate, (ii) the diffusion of active species to the interface and (iii) the thickness of very thin polymeric overlayers that remain on the substrate following failure. These aspects of the role of XPS in adhesion science have recently been reviewed [5].

XPS does, however, possess one well known shortcoming, which is its lack of spatial resolution. The standard, area integrating, analysis may originate from an area as large as $10mm^2$, but recent developments in the design of monochromated X-ray sources and position-sensitive analyser optics have brought micro-XPS a great deal closer. The importance of spatially-resolved XPS has been illustrated by several authors [6–8], and the development by Haack and co-workers [8] of an XPS mapping system (referred to by the authors as elemental mapping-XPS (EM-XPS)) has brought the chemical visualisation of the fracture surface to reality.

The use of imaging XPS methods, although invaluable for providing a view of localised changes in elemental surface composition, are invariably accompanied by a decrease in spectral resolution. Thus, in the present paper standard (area-integrating) XPS has been combined with the EM-XPS method developed by Haack and co-workers [8]. In addition, scanning electron microscopy and atomic force microscopy have been used to compare the morphology of the fracture surfaces of failed joints with that of the unbonded surfaces. Cross-sectional transmission electron microscopy has also been used to assess oxide thickness and to investigate the possibility of gross oxide degradation as a failure mechanism.

In Part III [2], the results presented in the earlier papers will be used to predict the lifetime of single-overlap joints subjected to cyclic fatigue loading.

2. EXPERIMENTAL

2.1. The Materials

The substrates employed were:

(i) An aluminium alloy (Grade: British Standard EN AW-5083) which contained 4.0 to 4.9 wt.% magnesium and 0.4 to 1.0 wt% manganese.
(ii) An electrogalvanised (EG) steel which was supplied in sheet form, with a thickness of 1.8 mm, by ACT Inc., USA. The galvanised coating on the surfaces of the steel sheet consisted of a zinc coating about 10 μm in thickness.

The adhesives employed were:

(i) A one-part epoxy-paste adhesive, Grade "XD4600" supplied by Ciba Polymers, UK. This adhesive had been especially developed for bonding aluminium alloys.
(ii) A one-part epoxy-paste, Grade "Terokal 4520-34" supplied by Teroson, Germany. This adhesive is currently being used to bond EG steel parts for the automobile industry.

2.2. Joint Preparation

2.2.1. The Aluminium-alloy/XD4600 Joints

The aluminium-alloy plate was either 11.0 mm or 12.7 mm in width and was machined, using a computer-controlled milling machine, into the tapered-cantilever beams. Before bonding, the substrates were either grit-blasted and solvent degreased (using 1,1,1 trichloroethane) or subjected to a chromic-acid etch [9].

Two pretreated aluminium-alloy beams were then bonded together to form a tapered-double cantilever-beam (TDCB) joint. A 90 mm length of release-coated aluminium foil was placed at the narrow end of the TDCB joint to act as a starter crack. The thickness of the adhesive layer was 0.4 mm and was controlled by the use of thin wires at the far ends of the TDCB joints. The adhesive was then cured by a two-stage heating process. The joints were initially placed in an oven pre-heated to 145°C for 10 minutes, after which the oven temperature

was raised to 190°C. It took about 15 minutes for the oven to reach 190°C, when the heaters were switched off and the joints were allowed to cool slowly overnight. A low pressure was applied to the joints during the adhesive curing process.

2.2.2. The EG Steel/Terokal 4250-34 Joints

The EG steel substrates were only available in relatively thin sheet form, and the sheet was far too thin to be used as beams for a double-cantilever beam (DCB) or TDCB specimens, since even under a relatively small load gross plastic deformation of the thin arms occurred. (Recall that a requirement for applying the methods of linear-elastic fracture-mechanics (LEFM) to analyse the measured test data is that the arms of the beam must exhibit only elastic deformation.) To overcome this problem, previous work by Jethwa *et al.* [10] has developed a "compound" TDCB specimen. In this novel type of specimen the thin EG steel is slotted and bonded into grooved tapered-double cantilever beams of aluminium-alloy, which act as support beams for the thin EG steel substrates. Two such "compound" beams are bonded together. The reader is referred to the previous publication [10] for further details of this "compound" TDCB joint specimen.

The coated surfaces of the EG steel were simply degreased using 1,1,1 trichloroethane prior to bonding. The adhesive employed was "Terokal 4520-34". A 90 mm length of release-coated aluminium foil was placed at the narrow end of the TDCB joint to act as a starter crack. The thickness of the adhesive layer was 0.4 mm and was controlled by the use of thin wire at the far ends of the TDCB joints. The adhesive was cured by heating to 180°C for 30 minutes, after which the oven heaters were switched off and the joints were allowed to cool slowly. A low pressure was applied to the joints during the adhesive curing process.

2.3. Joint Testing

The full details are given in Part I [1], so a short summary only is given here. To determine the adhesive fracture energy, G_c, using the adhesively-bonded TDCB, or compound TDCB specimens, tests were

conducted at a constant rate of displacement of the crosshead of the tensile testing machine. The rate of displacement used for these monotonically-loaded tests was 1.0 mm/min. The tests were conducted at $23 \pm 1°C$ and the relative humidity was 55 %.

The adhesively-bonded TDCB, or compound TDCB specimens, were also used to obtain the values of the rate of crack growth per cycle, da/dN, as a function of the maximum strain-energy release-rate, G_{max}, applied in the fatigue cycle. A sinusoidal loading waveform was employed at a frequency of 5 Hz. A range of maximum displacements, δ_{max}, was employed in order to cover the complete range of applied fracture energy, G_{max}, values; i.e. the range from $G_{max} \cong G_{th}$ up to $G_{max} \cong G_c$. The displacement ratio ($\delta_{ratio} = \delta_{min}/\delta_{max}$) was 0.5. For the tests conducted in the dry environment, the tests temperature was $23 \pm 1°C$ and the relative humidity was 55 %. For the tests conducted in the "wet" environment, the test temperature was $28 \pm 2°C$ and the joints were immersed in distilled water for about five minutes before the fatigue tests were started.

2.4. Surface Analysis

2.4.1. Introduction

The substrates prior to bonding and the fracture surfaces of the failed joints were analysed using various microscopy and surface analytical techniques.

2.4.2. Electron Microscopy

Samples for study using the scanning electron microscopy were mounted onto aluminium stubs using a double-sided tape and the perimeter of the sample was painted with "silver dag" to improve its electrical conductivity. To further prevent charging, the surface of the specimen was sputter coated with carbon. The samples were examined using a "JEOL JSM 5300" machine, using an accelerating voltage of 15 kV and an approximate working distance of 20 nm.

The main problem of using transmission electron microscopy stems from the need to use very thin specimens which can be penetrated by the electron beam. However, sectioning techniques have been

developed and used by Bishopp and co-workers [11, 12] for characterising the morphology at interfaces in aluminium bonded structures. Their techniques were followed in the present studies and involved firstly sputter-coating the surface with an impervious layer of gold-palladium and mounting the coated sample in an embedding resin. (These measures provided a clear indication of the locus of failure, since the failed region of the joint lay immediately below the sputter-coated layer, and they also prevented damage to the fracture surface during the later stages of specimen preparation.) The embedded specimens were cut perpendicular to the fracture surface using a "Reichart Ultracut" ultra-microtome system. The thickness of the microtomed slices was about 20 nm, and these were floated onto a microscope grid and examined using a "Philips EM 400" transmission electron microscope.

2.4.3. Atomic Force Microscopy (AFM)

The atomic force microscope senses the force between the apex of a sharp tip, attached to a cantilever spring and the atoms on the surface of the specimen, as the tip is scanned. These studies were conducted using a "Nanoscope III" system (Digital Instruments Inc., USA) in a "contact" mode under ambient conditions. Using a small saw, 3 mm thick samples were carefully cut from the substrates and mounted, using double-sided tape, onto a 15 mm steel disc. This was then placed on a electrically-grounded magnetic disc on top of a XYZ stage. The AFM tip was held stationery and the sample was scanned using piezoelectric transducers in the usual manner.

2.4.4. X-ray Photoelectron Spectroscopy (XPS)

XPS measurements were conducted using a "VG Scientific ESCALAB Mk II" spectrometer, interfaced to a "VGS 5000-S" data system based upon a "DEC PP 11/73" computer for data acquisition and analysis. Most spectra were excited using AlKα radiation, except for the fracture specimens with considerable XD4600 adhesive residues on them. These samples were analysed using MgKα radiation to avoid the superpositioning of Si photoelectron peaks with the Bremsstrahlung induced Al Auger peaks, which occurs with the former radiation

source. The specimens were mounted for analysis at an electron take-off angle of 45°, and the analysis was carried out at a base pressure of 10^{-7} Pa. The spectrameter was operated in the constant analyser energy mode. For survey spectra an analyser pass energy of 50 eV was used, whilst for high resolution spectra of the core XPS lines of interest (e.g. C1s, O1s, Al2p, Zn2p, Na1s, Si2p, Ca2p, N1s, etc.) a value of 20 eV was employed. The values of the binding energies are quated to an accuracy of ± 0.1eV and the values were corrected for electrostatic charging by setting the major component of the C1s peak to 285.0 eV.

2.4.5. *Elemental Mapping – X-ray Photoelectron Spectroscopy (EM-XPS)*

These studies used the method developed by Haack and co-workers [8] and employed a conventional small spot source (i.e. and X-ray beam diameter of about 600 μm) together with a computer-controlled sample stage. The software for control of the specimen stage during acquisition and the subsequent image processing routines to produce quantitative XPS maps was produced in-house by these workers. This technique of EM-XPS generates chemical-information maps of the failed surfaces from the joint (about 12.5 mm × 25.0 mm in total area) by alternating between collecting data and then moving the sample *via* the computer-controlled stage. The chemical-information map is generated by establishing sampling nodes every 0.4 mm in the Y-direction and 0.8 mm in the X-direction, i.e. the spatial resolution of the map is 0.4 mm × 0.8 mm. The total acquisition time for each map is approximately twenty-four hours and the detectable elements include C, O, Al, Zn, Na, Cl, Mg and Si. As may be seen clearly later, a colour scale consisting of bands of red, orange, yellow, green, blue indigo, violet and white, respectively, respresents the highest to the lowest concentration of an element detected. The detection threshold for the maps set at 2.0 at. % for each element. Also, in some cases, the conventional small spot (600 μm) X-ray source of the spectrometer was used in the static mode to obtain more complete small-area XPS analyses of regions of interest on the surfaces being studied.

3. RESULTS AND DISCUSSIONS

3.1. Analysis of Substrate and Adhesive Surfaces Prior to Bonding

3.1.1. Aluminium-alloy

XPS Studies The XPS survey spectra of the aluminium-alloy substrate surfaces before and after surface pretreatment are shown in Figures 1a to c for the "as-received", grit-blasted and degreased (GBD) pretreatment and the chromic-acid etched (CAE) pretreatment, respectively. The elemental compositions of the aluminium-alloys are given in Table II.

As may be seen from these results, the aluminium-alloy in the "as-received" state has a very high level of carbon contamination, and this attenuates most of the signal from the underlying substrate. This is not unusual for such a surface, as the high surface energy of the aluminium is likely to attract atmospheric contamination. Also, during milling of the arms of the TDCB specimen a protective organic cutting fluid is usually employed to prevent overheating and damage to the cutter, and the cutting fluid is another source for the carbon contamination. Obviously, if the carbon contamination is not largely removed prior to

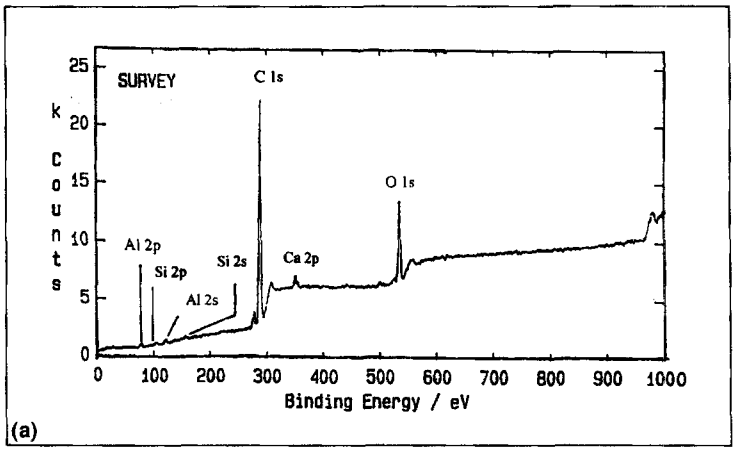

FIGURE 1 XPS survey spectra of the aluminium-alloys. (a) "As received". (b) Pretreated: grit-blasted and degreased (GBD). (c) Pretreated: chromic-acid etched (CAE).

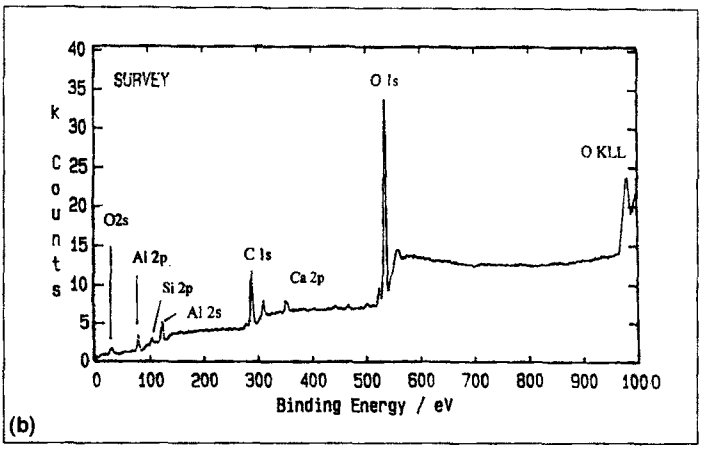

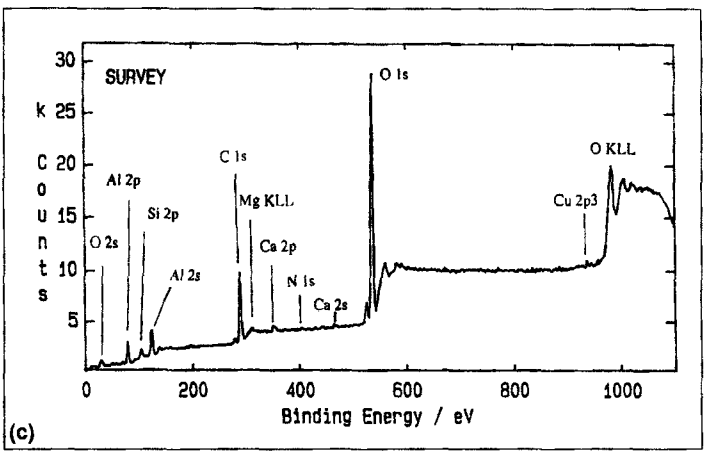

FIGURE 1 (Continued).

TABLE II Elemental compositions of the aluminium-alloy from the XPS studies (in atomic-%)

Treatment	*C*	*O*	*Al*	*N*	*Si*	*Cr*	*P*	*S*	*Fe*	*Cu*	*Ca*	*Mg*
"As-received"	81.3	14.4	3.3	n/d[a]	tr[b]	n/d	n/d	n/d	n/d	n/d	1.0	n/d
GBD	35.0	49.1	14.9	n/d	tr	n/d	n/d	n/d	n/d	n/d	1.0	n/d
CAE	30.0	44.3	16.0	1.2	4.7	0.6	1.8	0.4	n/d	tr	1.0	tr

[a]n/d: not detected.
[b]tr: trace.

bonding and/or adequately displayed by the adhesive, it may act as a "weak boundary layer", and so inhibit the formation of strong joints [13].

The use of a GBD pretreatment considerably reduces the level of the carbon contamination, whilst the use of the CAE pretreatment brings about an even greater reduction in the level of the carbon contamination. For both the GBD and the CAE pretreatments, the aluminium (Al2p) peak position was found to be at a binding energy of 74.3 ± 0.3 eV, and this corresponds to aluminium in the oxide form. Indeed, no aluminium in the metallic form (giving an Al2p peak position at about 72 eV) was detected on any of the aluminium-alloy surfaces. This indicates that the thicknesses of the oxide layers on the surfaces of the aluminium-alloys were greater than about 5 nm. This is consistent with the values of oxide thickness expected and reported by previous workers. For example, for the GBD pretreated aluminium-alloy, the thickness of the oxide layer would be expected to be of the order of a few nanometres. In the case of CAE pretreated aluminium-alloy, Kinloch and Smart [14] have previously estimated the oxide thickness to range from about 30 to 50 nm, from using argon-ion depth profiling coupled with XPS, and Bishopp and Thompson [12] have reported a value of about 30 nm from using TEM.

Considering the trace elements, then, although the CAE pretreatment is essentially a chromate solution, only relatively low concentrations of Cr (about 0.6%) were detected, together with a small concentration of phosphorus (about 2% present as a phosphate), sulphur (about 0.4% present as a sulphate) and silicon, about 5%. The absence of significant concentrations of chromates in the oxide of CAE-pretreated aluminium-alloy has previously been noted by several authors [14–16] and is thought to be due to the relatively large size of the chromate group, and hence its inability to be accommodated in the aluminium-oxide structure. Calcium is detected on all the aluminium-alloy surfaces and is most probably a contaminant from water washing of the materials.

AFM Studies The AFM image of the as-received aluminium-alloy clearly showed machine markings on the surface with a root mean square surface roughness, R_q, value of 15 nm. The GBD surface was far rougher with a R_q value of 65 nm. However, even for the GBD

surface there were no obvious topographical features which would permit mechanical interlocking of the adhesive with the oxide substrate. Instead, the surface appeared to be composed of open craters which were approximately 4 μm wide and 0.3 μm deep. In the case of the CAE-pretreated surfaces the value of R_q was about 50 nm and the surface appeared to be composed of open scallop-like features, as may be seen in Figure 2. The scallop-like features are about 1.8 μm across and 140 nm deep.

3.1.2. Electro-galvanised (EG) Steel

The XPS survey spectra of the EG steel substrate surfaces before and after surface pretreatment are shown in Figures 3a and b for the as-received and degreased pretreatment, respectively. The elemental compositions are given in Table III. As may be seen, degreasing the surface of the EG steel slightly decreases the concentration of the

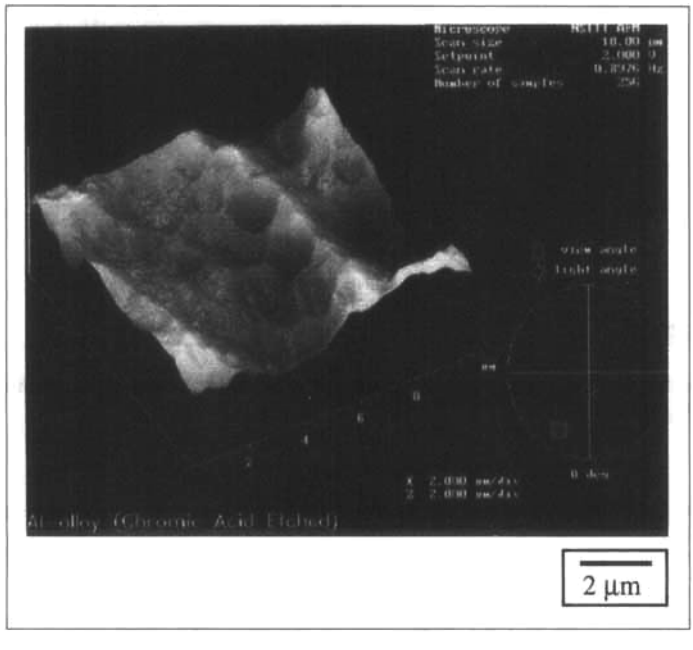

FIGURE 2 Atomic force microscopy (AFM) image of a chromic-acid etched (CAE) pretreated aluminium-alloy surface. (See Color Plate I).

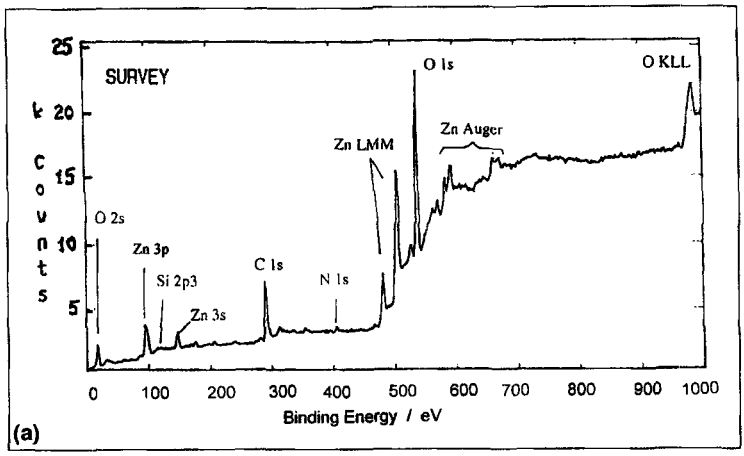

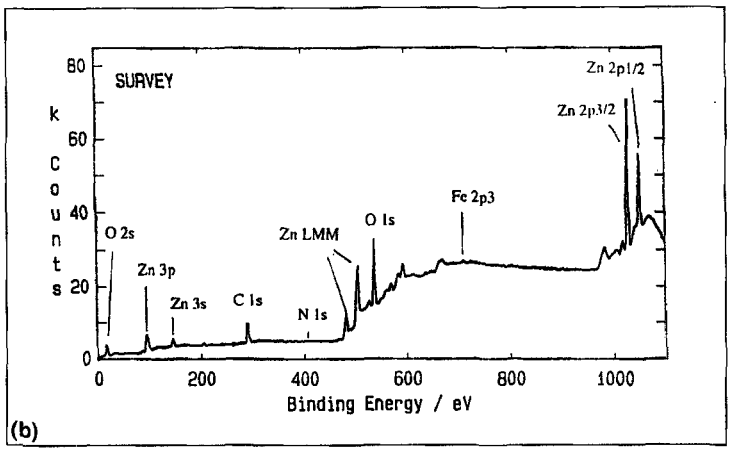

FIGURE 3 XPS survey spectra of the EG steel. (a) "As received". (b) Solvent degreased.

TABLE III Elemental compositions of the EG steel from the XPS studies (in atomic-%)

Treatment	*C*	*O*	*Al*	*N*	*Si*	*Cr*	*P*	*S*	*Zn*	*Fe*
"As-received"	37.5	40.7	n/d[a]	2.8	tr[b]	n/d	n/d	n/d	19.0	n/d
Degreased	35.8	36.5	n/d	1.3	tr	n/d	n/d	n/d	25.7	0.7

[a]n/d: not detected.
[b]tr: trace.

carbon contamination and significantly increases the level of zinc which is recorded. The zinc is present as zinc oxide. Since no significant levels of metallic zinc or iron are detected, the thickness of the zinc oxide is greater than 5 nm. Indeed, the thickness of the electro-galvanised layer is known to be of the order of micrometres.

3.1.3. Adhesive Materials

The XPS studies were undertaken on the (cohesive) fracture surfaces of the two adhesives in order to establish any "fingerprint" element which could be used later when the failing surfaces from the adhesive joints are examined. The XPS survey spectra of the "XD4600" and "Terokal 4520-34" adhesives are shown in Figures 4a and b, respectively. Both adhesives show the presence of the element nitrogen, which may be possibly be attributed to the curing agent. The element nitrogen is often considered to be a "fingerprint" element for use in the detection of any epoxy adhesive remaining on the fracture surface of an adhesive joint. However, in the present work there were small amounts of nitrogen present on the CAE pretreated aluminium-alloy and EG steel, see Tables II and III, respectively. The element silicon is also present in the adhesives, and may be arise from the presence of silica fillers or silane-coupling agents in the adhesives.

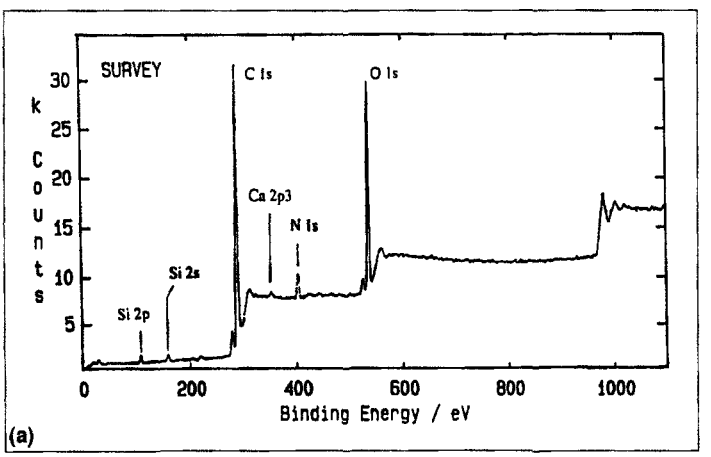

FIGURE 4 XPS survey spectra of the freshly-scrapped surfaces of the adhesives. (a) XD4600. (b) Terokal 4520-34.

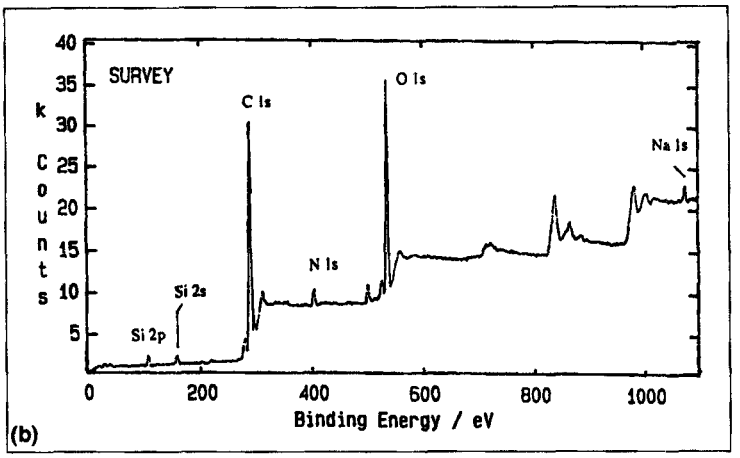

FIGURE 4 (Continued).

3.2. Locus of Failure Studies

3.2.1. Aluminium-alloy (GBD) Joints

Dry tests Visual inspection showed that, when the fracture tests were conducted in the relatively dry environment of $23 \pm 1°C$ and 55% RH on the joints prepared using the aluminium alloy which was subjected to a grit-blast and degrease (GBD) pretreatment prior to bonding, the locus of joint failure was mainly cohesive in the adhesive layer but with some apparent interfacial failure at the edges of the joint. This is stated in Table I and is shown in Figure 5.

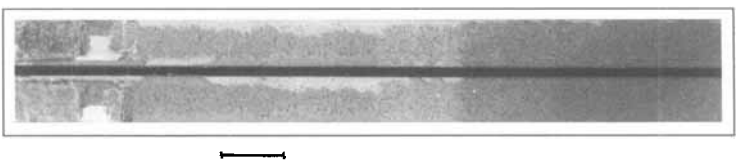

FIGURE 5 Photograph of the fracture surfaces of the aluminium-alloy (GBD pretreated) joint bonded using the XD4600 adhesive after "dry" fatigue testing. (The bar denotes where the specimen for the EM-XPS studies was taken, see Figure 6. The fatigue crack has propagated from left to right). (See Color Plate II).

The use of elemental mapping – X-ray photoelectron spectroscopy (EM-XPS) confirmed that the failure at the edges of the joint was indeed *via* a crack propagating along the adhesive/aluminium-oxide interface. Figure 6 illustrates the results from the EM-XPS studies. In this Figure, two photographs are given of the opposing halves of the fracture surfaces, taken from a specimen which had undergone fatigue testing in the "dry" environment. These two opposing halves of the fracture surfaces were actually cut from the specimen shown in Figure 5, and the bar marked on Figure 5 represents the location from where these two fracture surfaces were obtained. The XPS quantitative elemental maps for these two fracture surfaces are shown in Figure 6, as indicated on the figure. There are several noteworthy points. Firstly, the photographs in Figure 6 clearly show that over much of the joint the locus of joint failure was mainly cohesive in the adhesive layer, but with some apparent interfacial failure at, or close to, the edges of the joint. Secondly, within the resolution of the EM-XPS technique, there is no aluminium detected on the surface of the retained adhesive – even on those surfaces of the retained adhesive which corresponded to where apparent interfacial failure had occurred. This reveals that failure was not through the oxide layer. Thirdly, on what visually appears to be the aluminium-oxide surfaces, there are, indeed, relatively high concentrations of aluminium and oxygen, which indicates an aluminium-oxide surface. Fourthly, also, in these regions there is a substantially lower concentration of carbon, and this low concentration of carbon is typical of that associated with post-failure contamination of the aluminium oxide. These observations reveal that failure in these regions did not occur *via* fracture of the adhesive, even albeit close to the interface.

Thus, to summarise, the EM-XPS studies confirm that the locus of joint failure is mainly cohesive in the adhesive layer but with some adhesive/aluminium-oxide interfacial failure along the edges of the joint.

Wet tests For the tests conducted in the "wet" environment, the test temperature was $28 \pm 2°C$ and the joints were immersed in distilled water for about five minutes before the fatigue tests were started. Visually, the locus of joint was along the adhesive/aluminium-oxide interface, and no signs of gross corrosion of the substrate interface were observed. This is stated in Table I and shown in Figure 7.

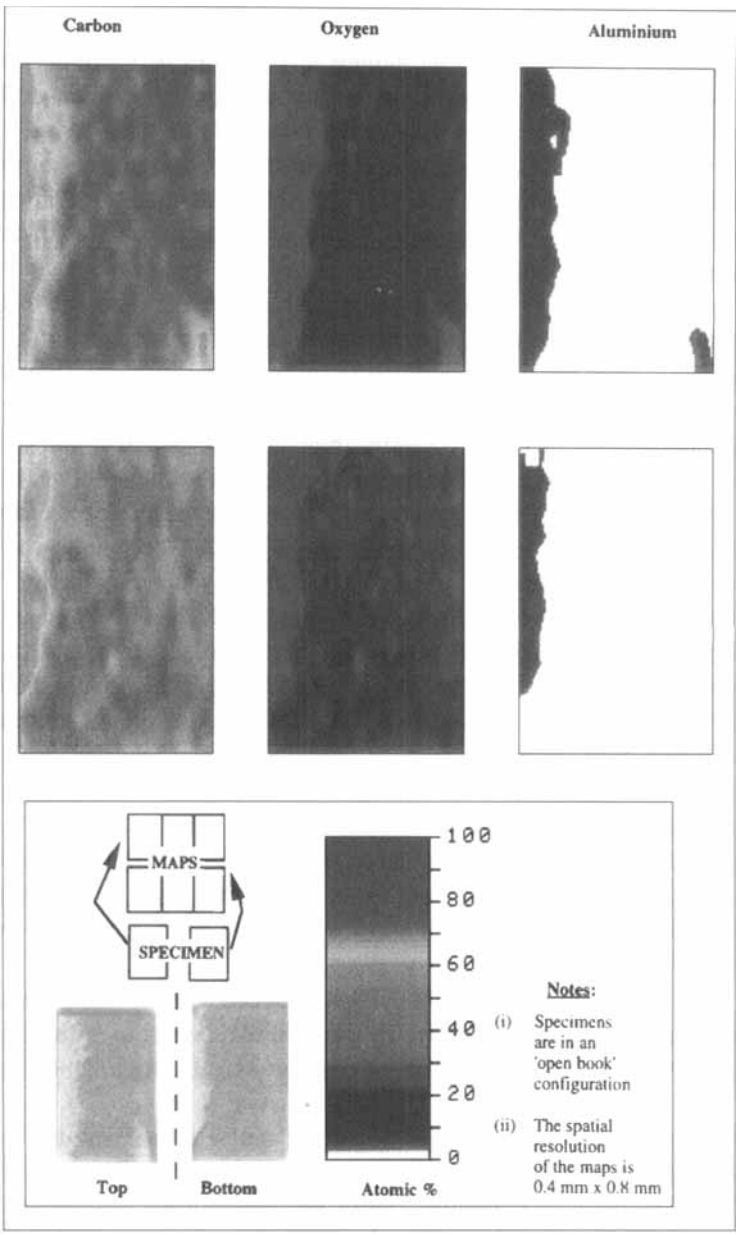

FIGURE 6 EM-XPS results for the fracture surfaces of the aluminium-alloy (GBD pretreated) joint bonded using the XD4600 adhesive after "dry" fatigue testing. (See Color Plate III).

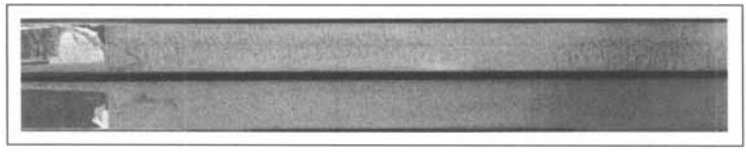

FIGURE 7 Photograph of the fracture surfaces of the aluminium-alloy (GBD pretreated joint bonded using the XD4600 adhesive after "wet" fatigue testing. (The fatigue crack has propagated from left to right.) (See Color Plate IV).

The XPS survey spectra are shown for the adhesive' side and for the metal side in Figures 8a and b, respectively; both spectra were recorded using MgKα radiation for the reasons outlined above. It may be clearly seen that there are aluminium signals on both fracture surfaces, and they are associated with aluminium oxide. However, if the results for the metal side of the failed joint (see Fig. 8b) are compared with those prior to bonding (see Fig. 1b), then the additional presence of nitrogen may be seen in Figure 8b. This nitrogen is likely to be associated with adhesive remaining on the metal side, as may be seen from comparing Figures 4a, 8a and 8b. Thus, it appears that the failure of the aluminium-alloy (GBD)/"XD4600"

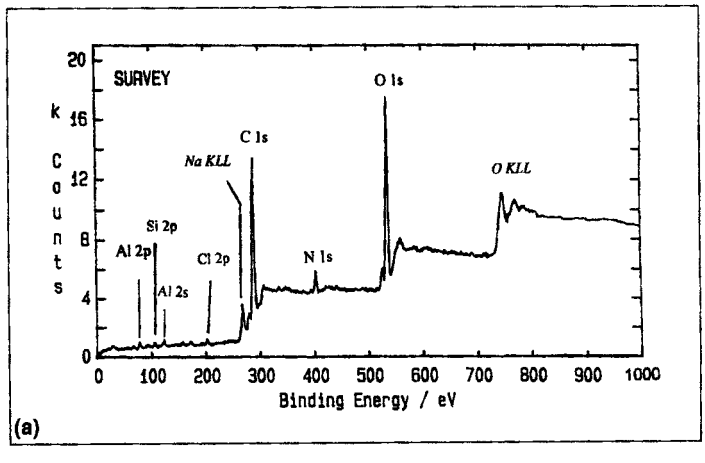

FIGURE 8 XPS survey spectra of the fracture surfaces of the aluminium-alloy (GBD pretreated) joint bonded using the XD4600 adhesive after "wet" fatigue testing. (a) Adhesive side (b) Metal side.

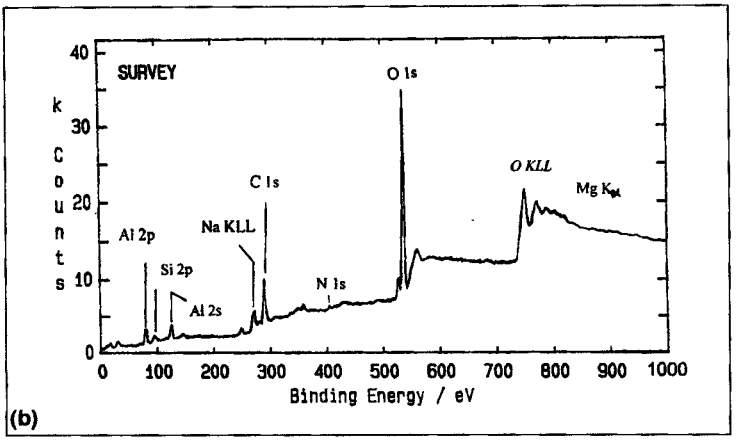

FIGURE 8 (Continued).

joints in the "wet" environment is complex with the crack propagating partially through the aluminium oxide, partially through the adhesive (but close to the interface) and, possibly, partially along the aluminium-oxide/adhesive interface. The sodium present undoubtedly arises from contamination of the fracture surfaces from sodium ions in the water, in which the joints were subjected to cyclic fatigue crack growth.

The results from the EM - XPS and detailed XPS spot-analyses also confirmed the above interpretations, but also added to these conclusions. These results clearly supported the fact that partial failure of the joint was *via* the fatigue crack travelling through the aluminium-oxide layer. These techniques indicated that, from the aluminium signal on the adhesive side, about 10 to 15% of the failure path was *via* crack propagation through the aluminium oxide and, from the nitrogen signal on the metal side, that about 25 to 20% of the failure was *via* fracture through the adhesive; the remaining 60 to 70% being *via* interfacial failure along the adhesive/aluminium-oxide interface. The most likely explanation for such a locus of failure is that the water attacks the interface, possible due to the disruption of the interfacial secondary bonds between the epoxy adhesive and the oxide [17, 18], and that the weakened interface now fails. The crack then travels along, or very close to, the interface. However, due to the relatively

high degree of surface roughness generated by the grit-blasting pretreatment, sometimes the fatigue crack passes through the top of an oxide asperity and sometimes passes through the adhesive which is filling the "valleys" between the oxide asperities, rather than follow the very tortuous path along the interface.

3.2.2. Aluminium-alloy (CAE) Joints

Dry tests Visual inspection showed that, when the fracture tests were conducted in the relatively dry environment of $23 \pm 1°C$ and 55% RH, the locus of joint failure was completely cohesive in the adhesive layer. This is stated in Table I. Therefore, as would be expected, the XPS survey spectra of both sides of the joint were identical to one another, and were identical to that shown previously in Figure 4a for a cohesive fracture surface of the "XD4600" adhesive.

Wet tests For the tests conducted in the "wet" environment, the test temperature was $28 \pm 2°C$ and the joints were immersed in distilled water for about five minutes before the fatigue tests were started. Visually, the locus of joint was along the adhesive/aluminium-oxide interface, and no gross corrosion of the substrate was observed. This is stated in Table I and may be seen from the photograph shown in Figure 9.

The XPS survey spectra for the adhesive side and for the metal side clearly revealed that there were aluminium signals on both fracture surfaces, and that they were associated with aluminium oxide. Nitrogen was present on the failed metal side of the joint. However, for the aluminium alloy which was CAE pretreated there was nitrogen present before bonding, as may be seen from Figure 1c. Thus, the

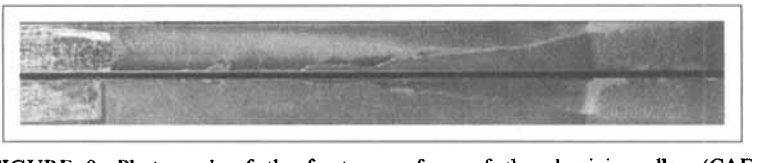

FIGURE 9 Photograph of the fracture surfaces of the aluminium-alloy (CAE pretreated) joint bonded using the XD4600 adhesive after wet fatigue testing. (The fatigue crack has propagated from left to right.) (See Color Plate V).

presence of nitrogen on the metal side cannot be taken to be indicative of the presence of adhesive remaining on the metal side of the joint. Neither sodium nor chlorine were detected on the failure surfaces. Although the fatigue tests were conducted in distilled water, there would be a low concentration of both sodium cations and chlorine anions available which could mark the sites of any cathodic or anodic corrosion activity. The absence of these ions from the fracture surfaces of the CAE-treated joints suggests that failure of the joint in the "wet" environment was not the result of an electrochemically-driven process.

The detailed XPS spot-analyses confirmed that aluminium was present on both sides of the failed joint. In the case of the metal side a concentration of 20 to 22% was detected and on the adhesive side a level of 16 to 17% was measured. Also, the carbon level was low, being 28 to 30% on the metal side and 33 to 38%, on the adhesive side.

The EM - XPS results are shown in Figure 10. These results clearly show the presence of aluminium covering the entire surfaces of both the metal side and the adhesive side of the failed aluminium-alloy (CAE)/"XD4600" joints. Also, in those regions of the adhesive side where the aluminium signal is relatively low, then the carbon signal is stronger. This suggests that the crack has propagated through the aluminium oxide, but not at a constant distance below the adhesive/aluminium-oxide interface. Thus, the conclusion is that fatigue testing in the "wet" environment leads to a locus of joint failure mainly through the oxide layer.

The techniques of atomic force microscopy and scanning electron microscopy supported the above conclusions but also revealed that there were scattered, isolated regions where adhesive remained on the metal side of the failed joints. Such regions represented only a very small fraction of the locus of failure, and the isolated regions of retained adhesive were only a few hundred micrometers in size.

Thus, the locus of failure for these joints when tested in the wet environment was *via* the fatigue crack propagating through the oxide layer, except for a few isolated regions where the crack wandered through the adhesive close to the interface.

As described previously, transmission electron microscopy was employed for characterising the morphology at the interfaces in the aluminium-alloy (CAE) joints. The technique involved firstly sputter-coating the fracture surface, from either the metal side or adhesive side

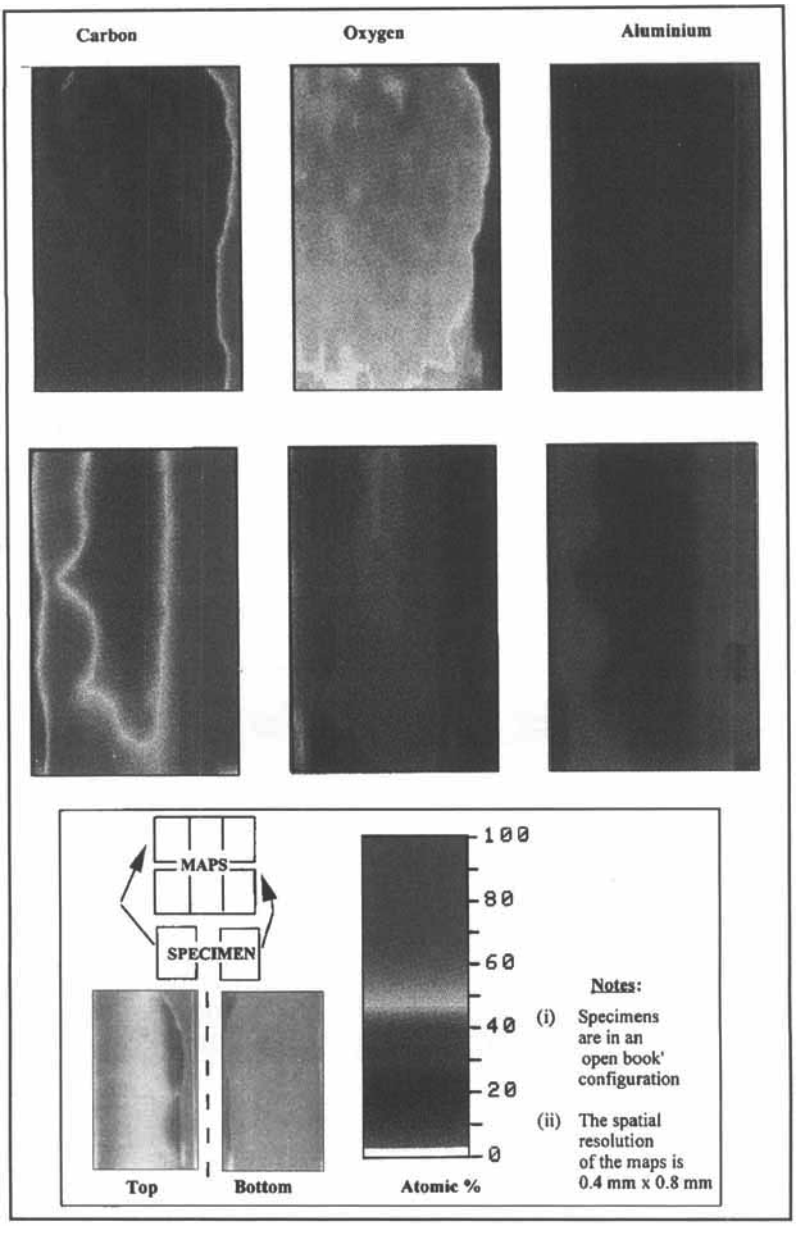

FIGURE 10 EM - XPS results for the fracture surfaces of the aluminium-alloy (CAE pretreated) joint bonded using the XD4600 adhesive after "wet" fatigue testing. (See Color Plate VI).

of the failed joint, with an impervious layer of gold-palladium and mounting the coated sample in an embedding resin. This provided a clear indication of the locus of failure, since the failed region of the joint lay immediately below the sputter-coated layer. The embedded specimens were cut perpendicular to the fracture surface using an ultramicrotome. The thickness of the microtomed slices was about 20 nm and these were floated onto a microscope grid and examined using a transmission electron microscope. The micrograph shown in Figure 11 is from a failed point, and a cross-section taken from the adhesive side is being viewed. As may be seen, the adhesive is covered by a layer of aluminium oxide, about 60 ± 30 nm in thickness. This is in complete agreement with the results from the various XPS studies. However, this information alone clearly does not yield the thickness of the aluminium-oxide layer at fracture, since some of the aluminium-oxide layer was retained on the metal side of the failed joint. However, the important question of the thickness of the oxide layer in the joints which were subjected to fracture *via* the wet fatigue test may be answered by considering Figure 12. This micrograph is again from a

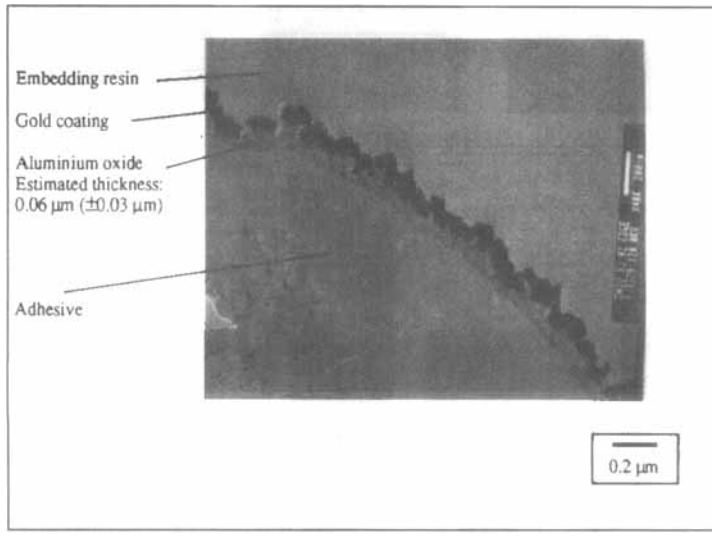

FIGURE 11 Transmission electron micrograph of a section through the adhesive side of the fracture surface of the aluminium-alloy (CAE pretreated) joint bonded using the XD4600 adhesive after "wet" fatigue testing. (The gold coating was placed on top of the original fracture surface to act as a marker.)

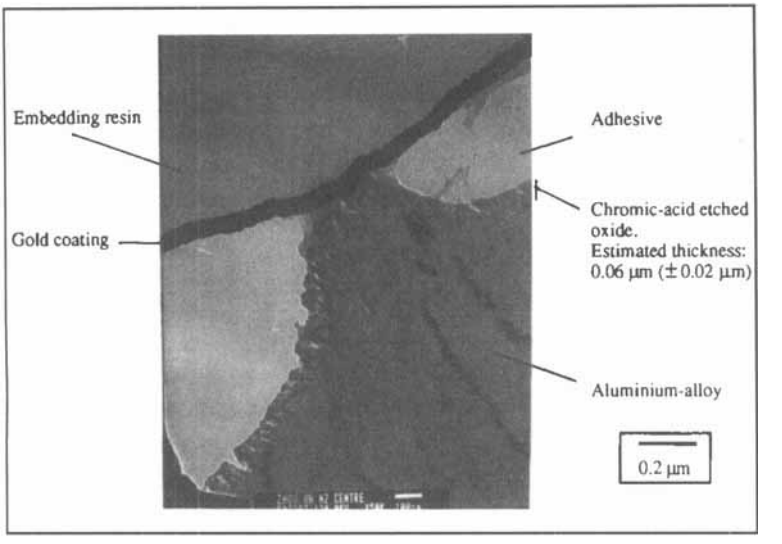

FIGURE 12 Transmission electron micrograph of a section through the metal side of the fracture surface of the aluminium-alloy (CAE pretreated) joint bonded using the XD4600 adhesive after "wet" fatigue testing. (The gold coating was placed on top of the original fracture surface to act as a marker.)

section of a joint which had been subjected to the wet fatigue test, but this section is taken from one of the isolated regions where adhesive has been retained on the metal side. Hence, the oxide layer thickness may be determined. The value is about 60 ± 20 nm. This value is very similar to that reported for the oxide initially produced by the chromic-acid etch (CAE) treatment and suggests that there has not been a major increase in the thickness of the oxide, due for example to a relatively gross corrosion mechanism occurring during the "wet" fatigue tests.

The above results show that neither (i) relatively gross corrosion nor (ii) a more subtle form of oxide hydration and thickening (both of which may lead to a weakening and failure of the oxide layer) are detected in the present work. The latter mechanism has been previously suggested [19], and supported by indirect evidence [20], but the present studies can find no direct evidence to support this hypothesis. The lack of direct evidence provided by the present work is in agreement with other recent studies [6, 12, 16].

Thus, to summarise, in the cyclic fatigue tests conducted in the "wet" environment using the aluminium-alloy (CAE pretreated)/"XD4600" joints the locus of failure is mainly through the aluminium-oxide layer, with just a few isolated instances where the crack has propagated through the adhesive, albeit very close to the interface. Of course, the important questions which arise are (i) why should the crack only travel through the oxide layer in the wet environment and, when is does so, (ii) why does the joint exhibit an inferior fatigue performance?. The obvious answer to both questions must be that the aluminium-oxide layer is mechanically weakened by the ingressing moisture, which reaches the interfacial regions of the joint *via* diffusion through the polymeric adhesive, and that these processes may occur relatively rapidly under the action of the cyclic fatigue stresses. However, this leads us to consider the mechanism for such a "weakening" effect. Firstly, we have shown that failure of these CAE-pretreated joints in the "wet" environment is not the result of an electrochemically-driven process. Thus, in agreement with previous workers, gross corrosion is not the usual form of failure mechanism. Secondly, as noted above, it has been suggested that the oxide layer generated by the CAE pretreatment may undergo hydration and a subsequent increase in thickness, which is accompanied by a loss of mechanical strength. Whilst such hydration is undoubtedly seen [16, 19, 20] on an exposed surface of the aluminium alloy, there is no evidence from the present transmission electron microscopy studies of such a change in the morphology of the oxide when covered by the adhesive layer in the joints. Thus, if such a mechanism does occur, it is very subtle in nature and beyond the resolution of the transmission or scanning electron microscopy studies. Hence, the details of the mechanism of attack by ingressing moisture on the oxide layer in the aluminium-alloy (CAE pretreated)/"XD4600" joints remains to be resolved.

3.2.3. EG Steel Joints

Dry tests In the case of the EG steel/"Terokal 4520-34" joints which were tested in the "dry" environment, the locus of failure was always *via* cohesive failure through the adhesive layer. This was evident from a simple visual examination, which was made particularly straightforward since the "Terokal 4520-34" adhesive was black in colour.

Wet tests For the tests conducted in the "wet" environment, the test temperature was $28 \pm 0°C$ and the joints were immersed in distilled water for about five minutes before the fatigue tests were started. Visually, the locus of joint failure was along the adhesive/zinc-oxide interface, as stated in Table I. In this case there were, however, signs of gross corrosion of the substrate. This was present as a white deposit on the adhesive side and the metal side of the failed joint, and may be clearly seen in the photographs of the two fracture surfaces shown in Figures 13a and 13b, respectively. This deposit was considered to be the corrosion product of zinc oxide, generally known as "white rust".

The XPS survey spectra are shown for the adhesive side and for the metal side in Figures 14a and b, respectively. The similarity of these two spectra is striking. There is a concentration of zinc (present as zinc oxide) of about 35 atomic-% on each side of the joint, with a rather low concentrations of carbon being recorded. The level of carbon on the metal side of the joint, see Figure 14b, is particularly low and is consistent with a voluminous (i.e. high surface area) corrosion product. The lack of sodium ions indicates that catholic conditions do not exist at this surface, but the EM - XPS data of Figure 13 show a low, but significant, concentration of chlorine. This element is presumed to be an impurity within the test medium but also serves the useful purpose of acting as a marker for corrosion (that is, the anodic dissolution of the metal). It is perhaps informative at this stage to describe, briefly, the use of marker ions in this manner, and relate such comments to the environmental degradation of EG steel.

It has been known for many years that the presence of ions from an electrolyte can give an indication of the prior electrochemical history of an electrode surface [21]. Thus, cations from the electrolyte solution (e.g. Na^+, Mg^{2+}) migrate to cathodic sites, whilst anions (e.g. Cl^-, SO_4^{2-}) migrate to anodic sites. This simple observation has been extremely useful in ahesion studies, since it has allowed the electrochemical conditions that have led to the failure of coating [22, 23] and adhesive joints [24 –27] to be deduced. In studies of low-carbon steels coated with a polymeric layer it is now well established that the exposed ("rusting") metal is anodic to the adjacent coated metal, at which the cathodic reduction of water and oxygen occurs to yield hydroxyl ions. This leads to alkaline conditions developing under the polymeric coating, which results in adhesion loss by a process

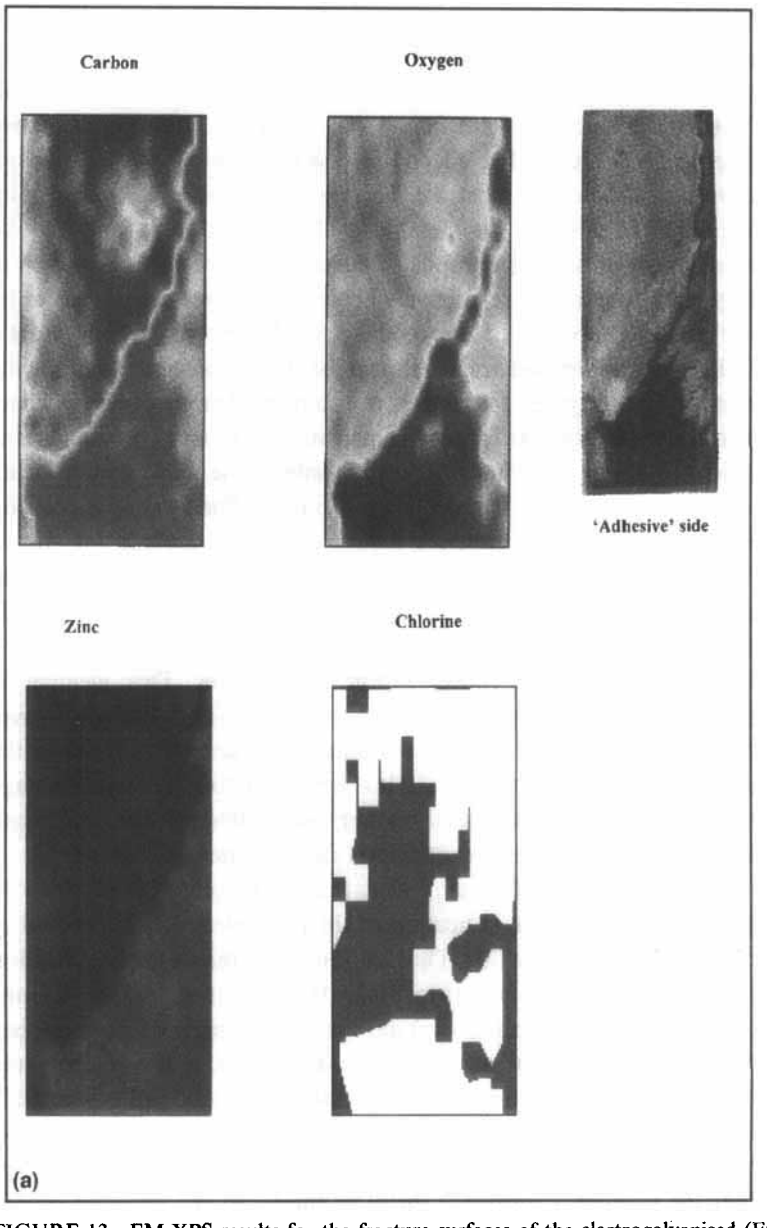

FIGURE 13 EM-XPS results for the fracture surfaces of the electrogalvanised (EG) steel joint bonded using the Terokal 4520-34 adhesive after "wet" fatigue testing. (a) Adhesive side (b) Metal side. (See Color Plate VII).

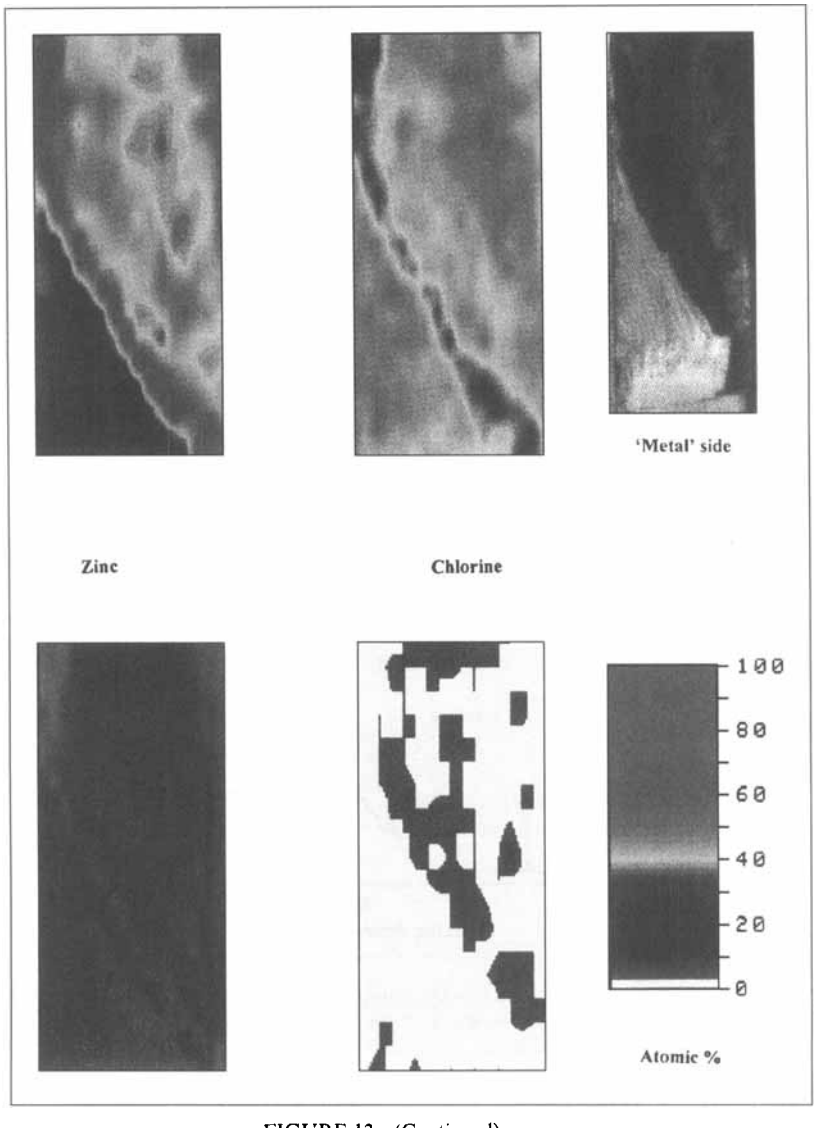

FIGURE 13 (Continued).

known as cathodic delamination, a phenomenon that has long been known [28] and that has been discussed by many authors [29–31]. In the case of adhesively-bonded zinc-coated (EG) steel, the process is

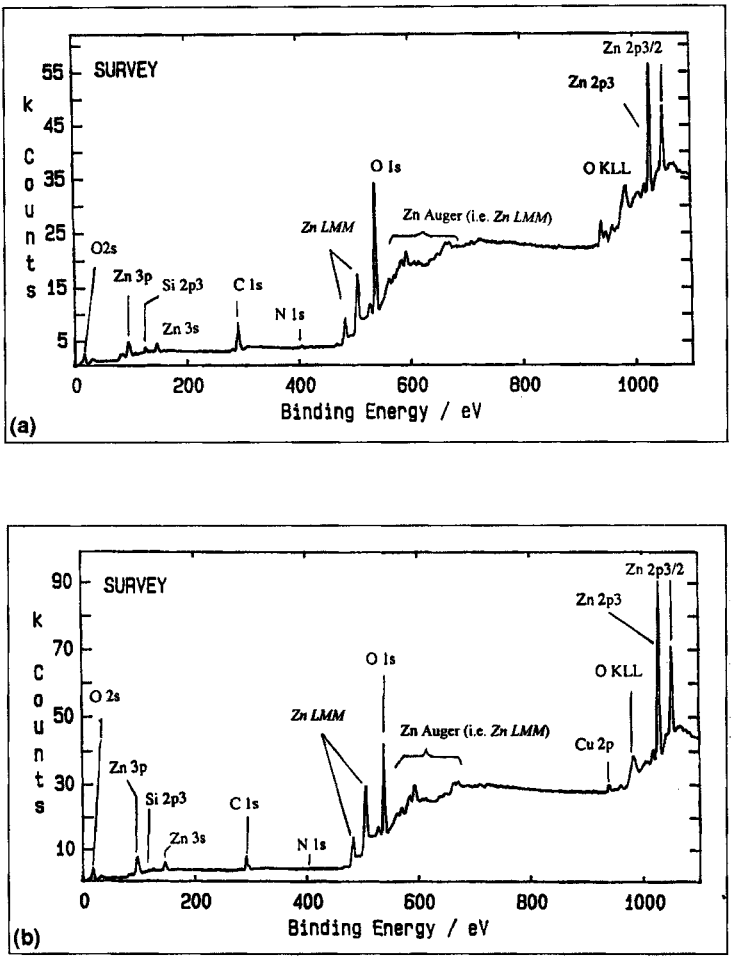

FIGURE 14 XPS survey spectra of the fracture surfaces of the electrogalvanised (EG) steel joint bonded using the Terokal 4520-34 adhesive after "wet" fatigue testing. (a) Adhesive side (b) Metal side.

somewhat more complex: the nature of the interfacial corrosion process is dependent on the state of mechanical loading during exposure. Provided that no mechanical load is applied to the specimens during corrosion exposure, bonded lap-shear specimens exposed periodically to salt water in a cyclic corrosion test exhibit an interfacial failure process that appears to be entirely anodic in

character. Corrosion of zinc at and near the interface is the dominant interfacial process [24–26]; the corresponding cathodic reaction presumably occurs at the exposed (steel) edges of the specimen. Similar experiments performed with specimens maintained under constant tensile load show a more complex pattern of interfacial corrosion processes, with an initially dominant anodic interfacial process supplemented shortly prior to spontaneous fracture by the formation of interfacial cathodic corrosion sites [8, 32].

Returning to the EM-XPS images of Figure 13, it is clear that the chlorine concentration is extremely low and, bearing in mind the poor photoelectric cross-section of the Cl2p core level, it is probably around the detection limit of XPS analysis in this form. Neither the (area-integrating) survey spectra of the metal side nor the adhesive side failure surfaces (see Fig. 14) indicate the presence of chlorine. This is consistent with sparsely-distributed regions of low concentration of chloride ions, which is the scenario indicated by the EM-XPS data. Thus, in terms of the chemistry of the failure process, the concentration of chlorine is so low that it can be excluded as a component of the reaction product, thus ruling out zinc chloride or basic zinc chloride. Another indication of the composition of the corrosion product is the carbonate group, since this may point to basic zinc carbonate. The C1s spectra of both failure surfaces do show the presence of a relatively minor concentration of carbonate ions, some 4.2 eV from the main peak. In the past, this has been suggested to arise from degradation of polymeric species [33], and the adsorption of these ions from aerated solution [34], in addition to the possibility of a major degradation product. Another possibility for the presence of carbonate species is that of post-failure degradation. However, whatever the source of the carbonate species, the concentration (about 5 atomic-%) of such groups is not sufficient to account for the high concentration of zinc ions, and the presence of carbonate ions is considered to be of relatively minor importance as far as the failure mechanism is concerned. Finally, no sodium ions were detected on either surface from the failed joints.

The EM-XPS data reinforce, and rationalise, the high concentration of zinc which is found to be present on both surfaces from the spectra shown in Figure 14. The physical images of the two regions examined by EM-XPS (Figs. 13a and 13b) both contain different coloured

regions which represent mirror-images of the metal side and the adhesive side of the failed joint. As expected, the higher concentration of zinc in the EM-XPS images is associated with the metal side of the failed joint. However, the main conclusion from Figure 14 is reinforced, namely that the adhesive side of the failed joint has a relatively high concentration of zinc completely covering the adhesive material. Furthermore, the concentration of zinc on this failure surface is much higher than would be expected if it were merely a result of the post-failure adsorption of corrosion products from solution. This observation, together with the chlorine analysis, the low concentration of carbon on both surfaces and the absence of sodium ions, indicates that failure is associated with gross corrosion, *via* anodic dissolution, of the zinc layer on the EG steel substrate.

The exact sequence of events leading up to the fatigue failure process can be envisaged in the following manner. Firstly, the joint edges (*i.e.* exposed steel) are cathodically protected by the anodic dissolution of the exposed zinc. Secondly, at the crack tip and environs, anodic activity occurs at the adhesive/metal (i.e. zinc oxide) interace, leading to the creation of a voluminous corrosion product with little cohesive strength. (Ready access of the exposure medium to the crack tip is ensured by the cyclic nature of the loading). Thirdly, as a result of the fatigue loading, the crack propagates close to the adhesive/zinc oxide interface, but within the corrosion deposit ("white rust"). Thus, subsequent surface analyses of both the metal side and adhesive side of the failed joint give spectra characteristic of the white rust degradation product. This is essentially the same observation as the result reported by Dickie *et al.* [26] for corrosion-induced adhesion loss of an epoxy adhesive on a galvanised steel in the absence of an applied tensile load. The white rust corrosion product is extremely fine in scale (perhaps of colloidal dimensions), and this aspect is confirmed by the atomic force microscopy studies described below.

From using both atomic force microscopy and scanning electron microscopy, it was readily confirmed that on both the adhesive side and the metal side of the failed EG steel joint there was a surface which had the distinct appearance of a metallic oxide. For example, Figures 15a and b show the images from AFM for the adhesive side and the metal side of a failed joint, respectively. The surface topography appears to be identical in both cases and, furthermore,

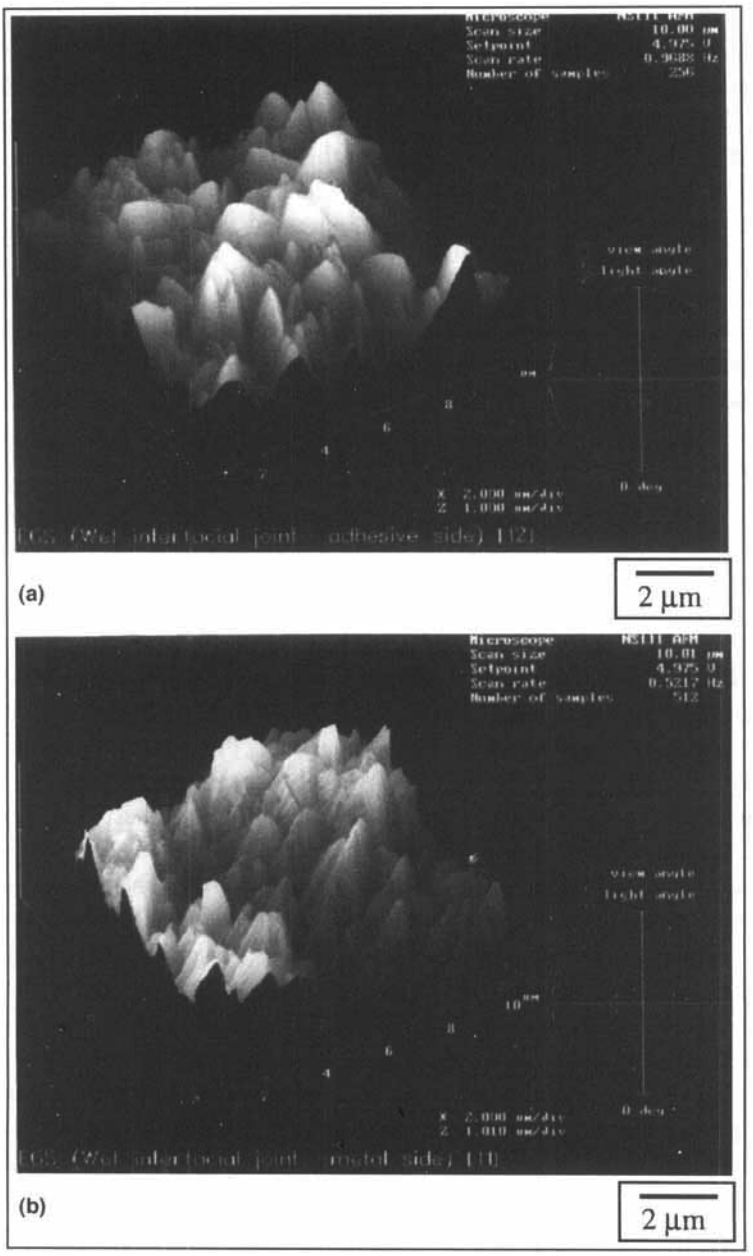

FIGURE 15 Atomic force microscopy (AFM) images of the fracture surfaces of the electrogalvanised (EG) steel joint bonded using the Terokal 4520-34 adhesive after "wet" fatigue testing. (a) Adhesive side. (b) Metal side. (See Color Plate VIII).

is identical to that of the EG steel surface prior to bonding, the needle-like columns on the surface being, from the XPS studies, zinc oxide.

Thus, the combination of microscopy and surface analysis suggests that the EG steel joints bonded using the "Terokal 4520-34" adhesive have failed in the "wet" fatigue tests *via* a crack propagating through a weakened zinc-oxide layer. As commented above, it is thought unlikely that failure simply occurs within the "bulk" of the original zinc coating, which is some 10 μm thick. It is considered that the mechanism of environmental failure involves anodic activity at the adhesive/metal (i.e. zinc oxide) interface, leading to the creation of a voluminous corrosion product with little cohesive strength, and that the fatigue crack propagates close to the adhesive/zinc oxide interface, but within the corrosion deposit (i.e. within the "white rust").

4. CONCLUSIONS

In Part [1] of the present series of papers, a fracture mechanics approach has been successfully used to examine the cyclic fatigue behaviour of adhesively-bonded joints, which consisted of aluminium-alloy or electro-galvanised (EG) steel substrates bonded using toughened-epoxy structural paste-adhesives. The adhesive systems are typical of those being considered for use, or in use, for bonding load-bearing components in the automobile industry. The results were plotted in the form of the rate of crack growth per cycle, da/dN, *versus* the maximum strain-energy release-rate, G_{max}, applied in the fatigue cycle, using logarithmic axes. The cyclic fatigue tests conducted in a relatively dry environment of 23°C and 55% r.h. were shown to cause crack propagation at far lower values of G_{max} compared with the value of the adhesive fracture energies, G_c, which were determined from monotonically-loaded fracture tests. Cyclic fatigue tests were also conducted in a "wet" environment, namely immersion in distilled water at 28°C. The "wet" fatigue tests clearly revealed the further significant effect an aggressive, hostile environment may have upon the mechanical performance of adhesive joints, and highlighted the important influence that the surface pretreatment, used for the substrates prior to bonding, has upon joint durability.

The present paper, Part II, has discussed the modes and mechanisms of failure for the two adhesive systems in both the "dry" and "wet" environments. The failure surfaces of the joints tested in Part I have been examined using a variety of analytical techniques and the surface chemistry and morphology compared with that of the "as prepared" (i.e. non-bonded) metal surfaces and cured adhesive. In the present investigation use has been made of an elemental mapping form of X-ray photoelectron spectroscopy (EM - XPS) along with conventional XPS. The surface topography has been examined using scanning electron microscopy and atomic force microscopy. Also, cross-sections of the joints have been studied using the transmission electron microscope. The results reveal that for both the aluminium alloy and EG steel joints the failure path is complex and, in the case of the latter

TABLE IV Summary of main results from present studies

Joint type	*Monotonic Tests*		*Fatigue tests*	
	$G_c(J/m^2)$	*LoF*	$G_{th}(J/m^2)$	*LoF*
Aluminium-alloy/ "XD4600" joints				
"Dry" environment:				
Grit-blast/degreased	3000	C(IF)[a]	250	C(IF)[a]
Chromic-acid etch	3500	C	355	C
"Wet" environment:				
Grit-blast/degrease	–	–	80	IF(Oxide/C)[b]
Chromic-acid etch	–	–	200	Oxide(C)[c]
EG steel/ "Terokal 4520-84" joints				
"Dry" environment:				
Degreased	740	C	240	C
"Wet" environment:				
Degreased	–	–	140	Zn[d]

[a]Mainly cohesive in the adhesive layer (C) but with some adhesive/aluminium-oxide interfacial failure (IF) along the edges of the joint.

[b]Failure at the adhesive/aluminium-oxide interface (IF) mainly occurs, possible due to the disruption of the interfacial secondary bonds between the epoxy adhesive and the oxide. However, due to the relatively high degree of surface roughness generated by the grit-blasting pretreatment, sometimes the fatigue crack passes through the top of an oxide asperity (Oxide) and sometimes passes through the adhesive (C) which is filling the "valleys" between the oxide asperities, rather than the crack following the very tortuous path along the interface.

[c]The crack propagated mainly through the aluminimum oxide (Oxide), except for a few isolated regions where the crack wandered through the adhesive (C) close to the interface. Neither (i) relatively gross corrosion nor (ii) a more subtle form of oxide hydration and thickening were detected in the present work.

[d]Failure in the electro-galvanised zinc coating (Zn) due to an electrochemically-driven (i.e. corrosion) mechanism.

joints when tested in the "wet" environment, is associated with electrochemical activity (i.e. corrosion). The main observations and conclusions are summarised in Table IV.

In Part III [2], the results presented in the earlier papers will be used to predict the lifetime of single-overlap joints subjected to cyclic fatigue loading.

Acknowledgements

The authors are pleased to acknowledge the suppport and sponsorship of this work by the Ford Motor Company and we would particularly like to acknowledge the assistance of Mr. P. A. Fay and Mr. R. E. Davis. We would also like to thank Professor G. Thompson (UMIST, UK) for his help with the preparation of the transmission electron microscopy specimens and Dr. P.A. Zhdan (University of Surrey, UK) for assistance with the atomic force microscopy studies.

References

[1] Jethwa, J. K. and Kinloch, A. J., *J. Adhesion* **61**, 71 (1997).
[2] Curley, A. J., Jethwa, J. K., Kinloch, A. J. and Taylor, A. C., *J. Adhesion*, this issue.
[3] Kinloch, A. J., *Proc. Inst. Mech. Engineers Preprints* **8**, 1 (1996).
[4] *Durability of Structural Adhesives*, A. J. Kinloch, (Ed.) (Applied Science Publishers, London, 1983).
[5] Watts, J. F., *In Problem Solving in Surface Analysis*, J. C. Riviere and S. Myhra (Marcel Dekker) (1997).
[6] Watts, J. F. Blunden, R. A. and Hall, T. J., *Surface and Interface Analysis* **16**, 227 (1990).
[7] van Ooij, W. J. Sabata, A. and Appelhans, D., *Surface and Interface Analysis* **17**, 403 (1991).
[8] Haack, L. P., DeBolt, M. A., Kaberline, S. L., deVries, J. E. and Dickie, R. A., *Surface and Interface Analysis* **20**, 115 (1993).
[9] Ministry of Defence, *Defence Specification* UK 03-2/1 (1970).
[10] Jethwa, J. K., Kinloch, A. J. and Wallington, G., *J. Materials Sci. Letters* **14**, 155 (1955).
[11] Bishopp, J. A., Sim, E. K., Thompson, G. E. and Wood, G. C., *J. Adhesion* **26**, 237 (1988).
[12] Bishopp, J. A. and Thompson, G. E., *Surface and Interface Analysis* **20**, 485 (1993).
[13] Brewis, D. M., *Int. J. Adhesion Adhesives* **13**, 251 (1993).
[14] Kinloch, A. J. and Smart, N. R., *J. Adhesion* **12**, 23 (1981).
[15] Cotter, J. L. and Kohler, R., *Int. J. Adhesion Adhesives* **1**, 23 (1980).
[16] Davies, R. J. and Kinloch, A. J., *In Adhesion-13*, K. W. Allen, Ed. (Elsevier Applied Sci., London), p. 8 (1989).
[17] Gledhill, R. A. and Kinloch, A. J., *J. Adhesion* **6**, 315 (1974).

[18] Kinloch, A. J., *Adhesion and Adhesives: Science and Technology* (Chapman and Hall, London), p. 350 (1983).
[19] Davis, G. D., Sun, T. S., Ahearn, J. S. and Venables, J. D., *J. Materials Science* **17**, 1807 (1995).
[20] Davis, G. D., Whisnant, P. L. and Venables, J. D., *J. Adhesion Sci. Technol.* **9**, 433 (1995).
[21] Castle, J. E. and Epler, D. C., *Surface Science* **53**, 286 (1975).
[22] Hammond, J. S., Holubka, J. W. and Dickie, R. A., *J. Coatings Technol.* **51**(655), 45 (1979).
[23] Watts, J. F. and Castle, J. E., *J. Materials Science* **18**, 2987 (1983).
[24] deVries, J. E., Holubka, J. W. and Dickie, R. A., *J. Adhesion Sci. Technol.* **3**, 189 (1989).
[25] deVries, J. E., Haack, L P., Holubka, J. W. and Dickie, R. A., *J. Adhesion Sci. Technol.*, **3**, 203 (1989).
[26] Dickie, R. A., Holubka, J. W. and deVries, J. E., *J. Adhesion Sci. Technol.* **4**, 57 (1990).
[27] Davis, S. J. and Watts, J. F., *J. Mater. Chem.* **6**, 479 (1996).
[28] Evans, U. R., *Trans. Electrochem. Soc.* **55**, 243 (1929).
[29] Dickie, R. A. and Smith, A. G., *Chemtech* **10**, 31 (1980).
[30] Leidheiser, H. Jr. and Wang, W., *J. Coatings Technol.* **53**(672), 77 (1981).
[31] Watts, J. F., *J. Adhesion*, **31**, 73 (1989).
[32] Dickie, R. A., DeBolt, M. A., Haack, L. P. and devries, J. E., *J. Adhesion Sci. Technol.* **8**, 1413 (1994).
[33] Holubka, J. W., Hommond, J. S. and Dickie, R. A., *Common Science* **21**, 239 (1981).
[34] Watts, J. F. and Castle, J. E., *J. Mater. Sci.* **19**, 2259 (1984).